ROYAL SOCIETY OF CHEMISTRY

CrossMark
← click for updates

# Shock wave studies of the pyrolysis of fluorocarbon oxygenates. I. The thermal dissociation of C₃F₆O and CF₃COF

C. J. Cobos,[a] K. Hintzer,[b] L. Sölter,[c] E. Tellbach,[c] A. Thaler[b] and J. Troe*[cd]

The thermal decomposition of hexafluoropropylene oxide, $C_3F_6O$, to perfluoroacetyl fluoride, $CF_3COF$, and $CF_2$ has been studied in shock waves highly diluted in Ar between 630 and 1000 K. The measured rate constant $k_1 = 1.1 \times 10^{14} \exp(-162(\pm 4) \text{ kJ mol}^{-1}/RT) \text{ s}^{-1}$ agrees well with literature data and modelling results. Using the reaction as a precursor, equimolar mixtures of $CF_3COF$ and $CF_2$ were further heated. Combining experimental observations with theoretical modelling (on the CBS-QB3 and G4MP2 *ab initio* composite levels), $CF_3COF$ is shown to dissociate on two channels, either leading to $CF_2 + COF_2$ or to $CF_3 + FCO$. By monitoring the $CF_2$ signals, the branching ratio was determined between 1400 and 1900 K. The high pressure rate constants for the two channels were obtained from theoretical modelling as $k_{5,\infty}(CF_3COF \rightarrow CF_2 + COF_2) = 7.1 \times 10^{14} \exp(-320 \text{ kJ mol}^{-1}/RT) \text{ s}^{-1}$ and $k_{6,\infty}(CF_3COF \rightarrow CF_3 + FCO) = 3.9 \times 10^{15} \exp(-355 \text{ kJ mol}^{-1}/RT) \text{ s}^{-1}$. The experimental results obtained at $[Ar] \approx 5 \times 10^{-6} \text{ mol cm}^{-3}$ were consistent with modelling results, showing that the reaction is in the falloff range of the unimolecular dissociation. The mechanism of secondary reactions following $CF_3COF$ dissociation has been analysed as well.

## 1. Introduction

While the pyrolysis of fluorocarbons, $C_xF_y$, and hydrofluorocarbons, $C_xF_yH_z$, has been studied extensively (see *e.g.* ref. 1), only little is known on the thermal dissociation of fluorocarbon oxygenates, $C_xF_yO_z$. The present series of investigations start to fill this gap. In the former reactions, complex elimination reactions with low energy barriers and comparably small preexponential factors of the high pressure rate constants were encountered in some cases. In other cases, the reactions were dominated by simple bond scissions with high energy barriers and large preexponential factors. It appears of interest to investigate whether the introduction of oxygen leads to similar observations.

We start the present work with a study of the decomposition of hexafluoropropylene oxide, $C_3F_6O$, which is known[2–7] to be a direct source of difluorocarbene, $CF_2$, by the reaction

$$C_3F_6O(+M) \rightarrow CF_3COF + CF_2(+M) \quad (1)$$

[a] *INIFTA, Facultad de Ciencias Exactas, Universidad Nacional de La Plata, Argentina*
[b] *Dyneon GmbH, Gendorf, D-84508 Burgkirchen, Germany*
[c] *Institut für Physikalische Chemie, Universität Göttingen, Tammannstrasse 6, D-37077 Göttingen, Germany. E-mail: jtroe@gwdg.de*
[d] *Max-Planck-Institut für Biophysikalische Chemie, Am Fassberg 11, D-37077 Göttingen, Germany*

In this way, reaction (1) behaves similar to the dissociation of perfluorocyclopropane,[8] $c\text{-}C_3F_6$, which is also a convenient source for $CF_2$ through the reaction

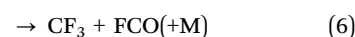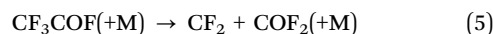$$c\text{-}C_3F_6(+M) \rightarrow C_2F_4 + CF_2(+M) \quad (2)$$
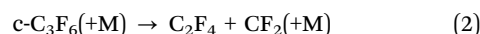
Reactions (1) and (2) both are characterized by limiting high pressure rate constants with low energy barriers and small preexponential factors. At the same time, they may be followed by the dimerization of $CF_2$ through[8–11]

$$CF_2 + CF_2(+M) \rightarrow C_2F_4(+M) \quad (3)$$
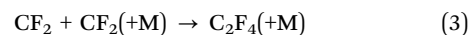
At higher temperatures, $C_2F_4$ from reaction (2) dissociates by the simple bond scission[11]

$$C_2F_4(+M) \rightarrow CF_2 + CF_2(+M) \quad (4)$$

with a much larger energy barrier and a larger preexponential factor. Not much is known on the corresponding reaction of perfluoroacetyl fluoride, $CF_3COF$, formed by reaction (1). IR multiphoton dissociation[12] suggested the primary process to be $CF_3COF \rightarrow C_2F_4 + O$. However, in view of the high endothermicity of this reaction channel and the indirect character of the experiments, this conclusion appears to be uncertain. Other pathways like
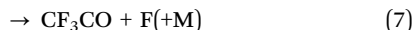
$$CF_3COF(+M) \rightarrow CF_2 + COF_2(+M) \quad (5)$$
$$\rightarrow CF_3 + FCO(+M) \quad (6)$$

This journal is © the Owner Societies 2017

*Phys. Chem. Chem. Phys.*, 2017, **19**, 3151–3158 | 3151

$$\rightarrow CF_3CO + F(+M) \tag{7}$$

on the basis of energy arguments should be more probable.

The present work investigated the dissociations of $C_3F_6O$ and $CF_3COF$ in shock waves by monitoring the UV absorption of $CF_2$. Because of the strong and well characterized properties of this absorption,[11] observations could be made over largely varying reaction conditions. At the same time, primary and secondary reactions could be distinguished. Like in our previous investigations of fluorocarbons and hydrofluorocarbons,[8,11,13–15] the experiments were accompanied by quantum-chemical calculations of the reaction pathways and theoretical modelling of the rate constants. This combination of experiment and theory is proved to be most advantageous again. Subsequent to the present work, a study of the decomposition of $C_4F_8O$ will be reported.[16]

## 2. Experimental technique and results

The thermal decomposition of $C_3F_6O$ was studied under high dilution by the bath gas M = Ar behind incident and reflected shock waves. The progress of the reaction was followed exclusively by the strong and quantitatively characterized UV absorption of $CF_2$ at 248 nm (with absorption coefficients[11] $\varepsilon(T)/cm^2\ mol^{-1} = 3.35 \times 10^6 + 4.6 \times 10^7 \exp(-[(T + 1457\ K)/1272\ K]^2) - 245(T/K)$, base e for $\varepsilon$). Details of our technique have been described before[8,11,13–15] and are only briefly summarized here. We used a shock tube of 9.4 cm inner diameter with a length of the test section of 4.15 m and of the driver section of 2.80 m. Windows for absorption measurements were placed 9 cm before the reflecting end plate. The light source was a Xe high pressure arc lamp (Osram XBO 150 W/4). A Zeiss MQ3 prism monochromator served for wavelength selection and signals were recorded using a multiplier (Hamamatsu E2420) – transient recorder arrangement. $C_3F_6O$ (from abcr, 97% purity) was mixed with Ar (from Air Liquide, 99.9999% purity) in large mixing vessels before the experiments. Mixtures with about 500 and about 50 ppm in Ar were prepared. The concentration of $C_3F_6O$ in the mixtures was controlled by the amount of $CF_2$ formed behind the shock waves. For the 500 ppm mixtures, the concentration of $CF_2$ in the experiments on reaction (1) was equal to the nominal value from mixture preparation. For the 50 ppm mixtures, some wall adsorption occurred in the vessel and in the shock tube before the experiments. This loss of $C_3F_6O$, however, could easily be accounted for, again from the $CF_2$ yield in low temperature experiments where one $CF_2$ is formed per one $C_3F_6O$ decomposed. The accurate determination of the starting concentration of $C_3F_6O$ at various places of the analysis was essential, see below.

### 2.1 Dissociation of $C_3F_6O$ and dimerization of $CF_2$

The formation and consumption of $CF_2$ in reactions (1) and (3) at a comparably low temperature of 800 K is illustrated in Fig. 1. While the formation of $CF_2$ by reaction (1) corresponds to a first order process, $CF_2$ disappears in the second order process of reaction (3), resulting in absorption–time profiles such as shown in the figure. Contributions from other reactions like $C_3F_6O \rightarrow C_2F_4 + COF_2$ or $C_3F_6O \rightarrow CFCF_3 + COF_2$, such as
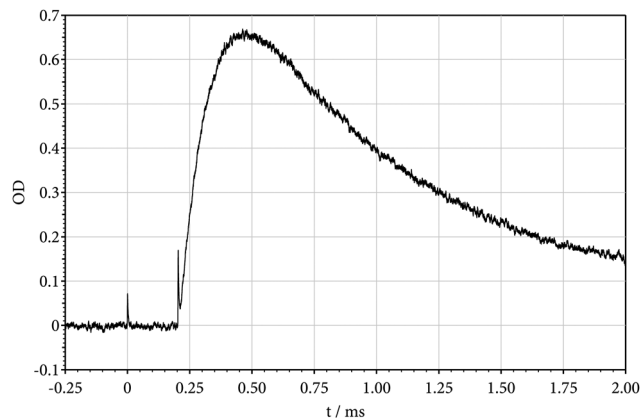


Fig. 1 Absorption–time profile of $CF_2$ at 248 nm in dissociation $C_3F_6O \rightarrow CF_3COF + CF_2$ followed by dimerization $2CF_2 \rightarrow C_2F_4$ behind a reflected shock wave ($T = 801$ K, [Ar] = $7.8 \times 10^{-5}$ mol cm$^{-3}$, relative reactant concentration $[C_3F_6O]_{t=0}/[Ar] = 5.1 \times 10^{-4}$; optical density OD $\propto [CF_2]$, see the text; Schlieren peaks indicating the arrival of the incident and reflected shock wave).

observed in multiphoton dissociation[17] of $C_3F_6O$, were not noticed (as deduced from the observation of one $CF_2$ formed per one $C_3F_6O$ decomposed under low temperature conditions). Since reaction (1) has a much stronger temperature dependence than reaction (3), by increasing the temperature one can accelerate reaction (1) to such an extent that clean second order absorption–time profiles for $CF_2$ dimerization become observable. This is illustrated in Fig. 2 for an experiment at 1100 K behind the reflected shock. On the other hand, by lowering the reactant concentration the second order dimerization can be slowed down to such an extent that the absorption–time profile of $CF_2$ is dominated by a clean first-order profile from reaction (1). This is shown in Fig. 3 by an experiment with 35 ppm of $C_3F_6O$ in Ar, instead of about 500 ppm of Fig. 1 and 2. Signals like Fig. 3 were represented by
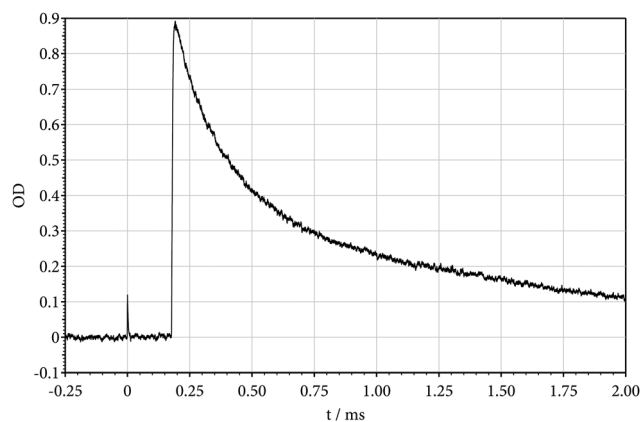
$$[CF_2] = [C_3F_6O]_{t=0}\{1 - \exp(-k_1 t)\} \tag{8}$$

and signals like Fig. 2 by



Fig. 2 As Fig. 1, showing dominant dimerization $2CF_2 \rightarrow C_2F_4$ at higher temperature ($T = 1103$ K, [Ar] = $5.5 \times 10^{-5}$ mol cm$^{-3}$, $[C_3F_6O]_{t=0}/[Ar] = 5.3 \times 10^{-4}$).

3152 | *Phys. Chem. Chem. Phys.*, 2017, 19, 3151–3158

This journal is © the Owner Societies 2017
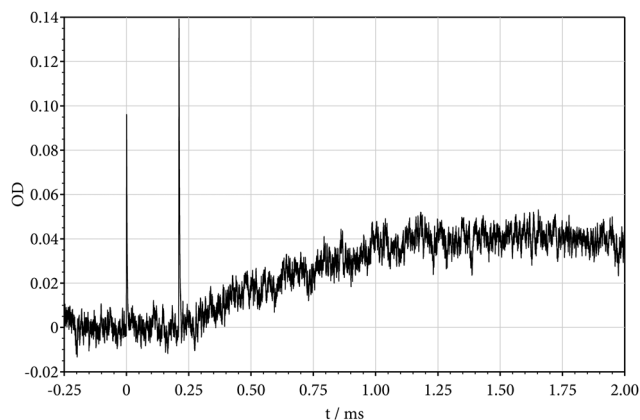
**Fig. 3** As Fig. 1, showing dominant dissociation $C_3F_6O \rightarrow CF_3COF + CF_2$ at lower temperature and lower reactant concentration ($T$ = 728 K, [Ar] = $8.7 \times 10^{-5}$ mol cm$^{-3}$, $[C_3F_6O]_{t=0}$/[Ar] = $3.5 \times 10^{-5}$).

$$1/[CF_2] - 1/[C_3F_6O]_{t=0} = 2k_3 t \qquad (9)$$

Numerical fitting of signals like Fig. 1 led to $k_1$ and $k_3$ simultaneously. Table 1 summarizes the resulting $k_1$ together with the applied experimental conditions while Fig. 4 illustrates the temperature dependence of $k_1$. We note that the reactant concentrations were varied by about a factor of 15. By measuring $k_1$ behind incident and reflected waves, the bath gas concentration [Ar] was varied by about a factor of 20. Within this variation no dependence of $k_1$ on [Ar] was noticed such that reaction (1) was found to be very close to the high pressure limit of the unimolecular dissociation. This is in accord with our modelling results (see below). The temperature dependence of $k_1$, as illustrated by Fig. 4, is well represented by

$$k_1 = 1.1 \times 10^{14} \exp(-162(\pm 4)\text{kJ mol}^{-1}/RT) \text{ s}^{-1} \qquad (10)$$

**Table 1** Rate constants $k_1$ for dissociation $C_3F_6O \rightarrow CF_2 + CF_3COF$ (experiments in Ar with $[C_3F_6O]_{t=0}$/[Ar] $\approx 5 \times 10^{-4}$)

| $T$/K | [Ar]/$10^{-5}$ mol cm$^{-3}$ | $k_1$/s$^{-1}$ |
|---|---|---|
| 628 | 9.7 | $4.3 \times 10^0$ |
| 632 | 10.0 | $3.5 \times 10^0$ |
| 659 | 9.9 | $1.9 \times 10^1$ |
| 670 | 9.1 | $2.9 \times 10^1$ |
| 677 | 2.4 | $3.5 \times 10^1$ |
| 692 | 9.2 | $7.0 \times 10^1$ |
| 694 | 8.9 | $8.9 \times 10^1$ |
| 696 | 8.6 | $9.1 \times 10^1$ |
| 715 | 2.3 | $1.8 \times 10^2$ |
| 739 | 8.5 | $4.1 \times 10^2$ |
| 744 | 2.1 | $5.1 \times 10^2$ |
| 751 | 1.9 | $6.5 \times 10^2$ |
| 753 | 8.0 | $7.9 \times 10^2$ |
| 763 | 2.0 | $9.7 \times 10^2$ |
| 764 | 8.1 | $1.0 \times 10^2$ |
| 783 | 6.9 | $1.3 \times 10^3$ |
| 801 | 7.8 | $2.1 \times 10^3$ |
| 805 | 1.8 | $2.8 \times 10^3$ |
| 824 | 1.7 | $4.7 \times 10^3$ |
| 861 | 1.5 | $2.0 \times 10^4$ |
| 888 | 1.5 | $3.1 \times 10^4$ |
| 918 | 1.4 | $5.1 \times 10^4$ |
| 945 | 1.3 | $9.2 \times 10^4$ |
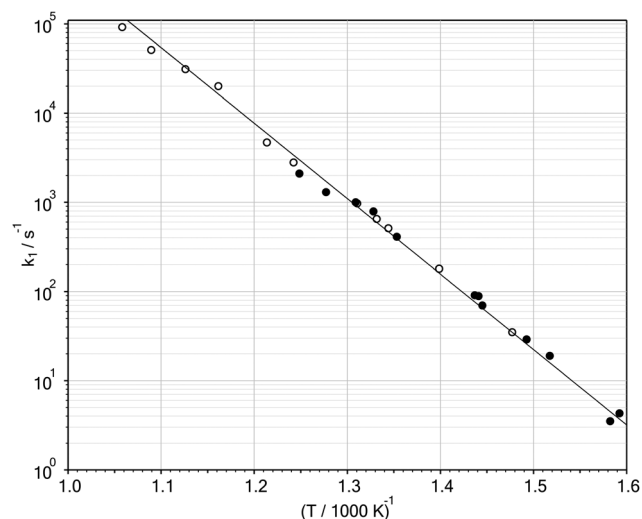


**Fig. 4** Rate constants $k_1$ for $C_3F_6O$ dissociation (from present work; $\bigcirc$: [Ar] = $(1-2) \times 10^{-5}$ mol cm$^{-3}$, $\bullet$: [Ar] = $(5-10) \times 10^{-5}$ mol cm$^{-3}$; the line corresponds to a linear fit of the points).

**Table 2** Rate constants $k_3$ for dimerization $2CF_2 \rightarrow C_2F_4$ (rate law d[CF$_2$]/dt = $-2k_3$[CF$_2$]$^2$, experiments in Ar with $[C_3F_6O]_{t=0}$/[Ar] $\approx 5 \times 10^{-4}$)

| $T$/K | [Ar]/$10^{-5}$ mol cm$^{-3}$ | $k_3$/$10^{10}$ cm$^3$ mol$^{-1}$ s$^{-1}$ |
|---|---|---|
| 739 | 8.5 | 7.2 |
| 753 | 8.0 | 7.2 |
| 764 | 8.1 | 7.2 |
| 897 | 7.0 | 8.6 |
| 940 | 6.5 | 8.1 |
| 978 | 5.9 | 6.8 |
| 1109 | 1.0 | 4.1 |

The modelling results of the present work and the previous results from ref. 5–7 are compared with eqn (10). The general agreement was found to be most satisfactory such that $k_1$ is well established now between 410 K (from ref. 5) and about 1000 K from the present work. (We note that $k_1$ was measured in pure $C_3F_6O$ in ref. 5–7 while the present experiments were performed under high dilution of $C_3F_6O$ in Ar.)

In contrast to $k_1$, $k_3$ depends both on the temperature and the bath gas concentration [Ar]. Table 2 summarizes the derived $k_3$ as a function of $T$ and [Ar]. The data clearly indicate that reaction (3) under the present conditions is in the intermediate range between a low pressure third order and a high pressure second order combination reaction. This is consistent with the earlier results for the dimerization from ref. 8–10 and the results for the reverse thermal dissociation (4) from ref. 11. Fig. 5 demonstrates this behaviour by including the present results into the representation of $k_3$ ($T$, [Ar]) from ref. 8 at two representative values of [Ar].

## 2.2 Dissociation of CF$_3$COF

After the dissociation of $C_3F_6O$ by reaction (1) is complete, one may study the subsequent dissociation of the reaction product $CF_3COF$. In the present case, equimolar mixtures of $CF_3COF$ and $CF_2$ formed by reaction (1) are studied at temperatures
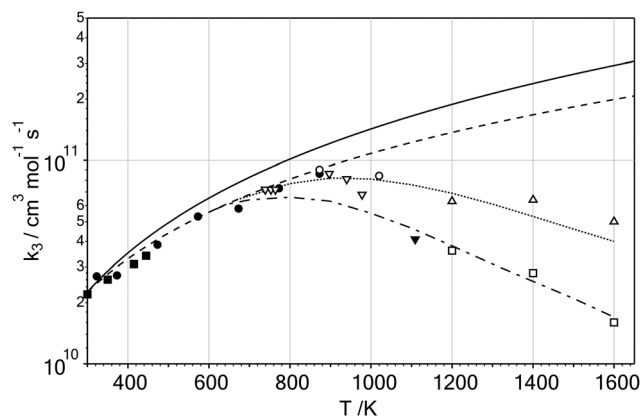
This journal is © the Owner Societies 2017

*Phys. Chem. Chem. Phys.*, 2017, **19**, 3151–3158 | **3153**

Fig. 5 Rate constants $k_3$ for $CF_2$ dimerization (see Fig. 6 of ref. 8; present work: $\triangledown$: [Ar] $\approx 5 \times 10^{-5}$ mol cm$^{-3}$, $\blacktriangledown$: [Ar] $= 1 \times 10^{-5}$ mol cm$^{-3}$; results from $C_2F_4$ dissociation:[11] $\triangle$: [Ar] $\approx 5 \times 10^{-5}$ mol cm$^{-3}$, $\square$: [Ar] $\approx 1 \times 10^{-5}$ mol cm$^{-3}$; results from ref. 8: $\bigcirc$: [Ar] $\approx 5 \times 10^{-5}$ mol cm$^{-3}$; results from ref. 10: $\bullet$: in 1 bar of Ar; results from ref. 10: $\blacksquare$: in 50 Torr of $N_2$; full and dashed lines: high pressure limit of $k_3$ from ref. 8 and 11; dotted line: $k_3$ at $5 \times 10^{-5}$ mol cm$^{-3}$ and dash-dotted line: $k_3$ at $1 \times 10^{-5}$ mol cm$^{-3}$ from ref. 8).



Fig. 6 Concentration–time profile of $CF_2$ at 248 nm, showing $CF_2$ formation from $CF_3COF$ dissociation behind incident shock ($T_2 = 1836$ K and [Ar]$_2 = 4.1 \times 10^{-6}$ mol cm$^{-3}$) and $CF_2$ dissociation behind reflected shock ($T_5 = 3930$ K, [Ar]$_5 = 9.5 \times 10^{-6}$ mol cm$^{-3}$) (the vertical axis corresponds to the $CF_2$ yield $Y(CF_2) = [CF_2]/[C_2F_6O]_{t=0}$) for the reaction behind the incident shock; the time scale for the reaction behind the incident shock is compressed by a factor of 3.39, see the text).

considerably higher than those employed in the experiments described in Section 2.1. The shock wave experiment now is conducted in three stages. Behind the incident wave, first, reaction (1) occurs so rapidly that, at the arrival of the shock front, there is an absorption step arising from the primarily formed $CF_2$. The $CF_2$ yield, $Y(CF_2)$ (defined by $Y(CF_2) = [CF_2]/[C_3F_6O]_{t=0}$), in this step increases from 0 to unity. Second, during a subsequent dissociation of $CF_3COF$ by reactions (5) and (6), $Y(CF_2)$ further increases; the rate of this increase and the level of the reached $Y(CF_2)$ provide access to $k_5$ and $k_6$. Finally, when the reaction mixture is further heated and compressed in the reflected shock wave, $CF_3$ formed in reaction (6) first rapidly decomposes to $CF_2$ and F, before all $CF_2$ from the various reactions decomposes at the now very high final temperature. Fig. 6 shows an example for the time dependence of the $CF_2$ absorption signal such as recorded during this three-stage experiment. In order to convert the $CF_2$ absorption into concentrations, one has to account for the changes in gas density and temperature (and, from the latter, the $CF_2$ absorption coefficient) in the incident and reflected wave. For the most relevant incident shock wave here, in Fig. 6 the $CF_2$ absorptions have been converted to the yields $Y(CF_2)$ and given by the vertical axis. On the other hand, the horizontal axis corresponds to the laboratory time. For the stationary gas behind the reflected shock, like in Fig. 1–3, also in Fig. 6 this corresponds to the time scale of the reacting species. In Fig. 6 the decay of the $CF_2$ signal at a temperature of 3930 K of the reflected shock then follows exactly the expected result for $CF_2$ decomposition from ref. 18. Evaluating the kinetics behind the incident shock, one has to account for the fact that the shock heated gas here flows towards the reflecting end plate of the shock tube. As is well known, the apparent "compression of the laboratory time" in comparison to the reaction time then corresponds to the density ratio across the incident shock front which, in the experiment of Fig. 6, amounts to a factor of 3.39.
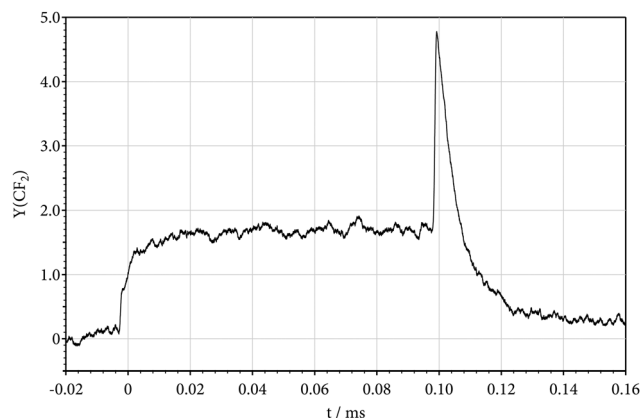
The observed time dependence of $Y(CF_2)$ behind the incident wave in this way leads to the sum of $k_5$ and $k_6$ while the reached level of $Y(CF_2)$ corresponds to the ratio $k_5/(k_5 + k_6)$. Experiments as shown in Fig. 6 could be done at temperatures behind the incident shock between 1400 and 1900 K at [Ar] $\approx 5 \times 10^{-6}$ mol cm$^{-3}$. The results, e.g. $k_5 \approx 5 \times 10^2$, $9.4 \times 10^3$, and $6.4 \times 10^4$ s$^{-1}$ for $T = 1410$, 1590, and 1840 respectively, were found to be about a factor of 2 to 5 smaller than modelled high pressure values of $k_5$ given below. We attribute this observation to falloff effects which should become visible for the higher temperatures and a smaller molecular size of $CF_3COF$ compared to the $C_3F_6O$ experiments. In this way, the two dissociation channels of $CF_3COF$ should behave similar to the dissociation of $C_2F_6$ for which falloff effects were analysed in ref. 19. Falloff curves for reactions (5) and (6) were characterized with the data modelled below and represented in the Appendix.

### 2.3 High temperature reaction mechanism

Fig. 6 corresponds to an experiment with very high temperatures behind the reflected shock such that $CF_2$ dissociates thermally. When lower temperatures were generated in the reflected shock, the situation changed because then a mechanism of unimolecular and bimolecular reactions was found to influence the observed $CF_2$ absorption–time profiles. Varying the reactant concentration allows one to distinguish between first and second order processes. First, we look at low-concentration experiments with about 40 ppm of $C_3F_6O$ in Ar. Fig. 7 illustrates the formation of $CF_2$ by reaction (1) at 770 K behind the incident wave. At the temperature of the reflected wave of 1380 K, that part of the initial $C_3F_6O$ which has not yet reacted at the arrival of the reflected wave decomposes almost instantaneously to $CF_3COF$ and $CF_2$. For the conditions of Fig. 7, reaction (3) is too slow to occur. Systematically exploring the absorption steps at the arrival of the reflected wave, however, reveals that more $CF_2$ is present than corresponds to unity yield $Y = 1$ from
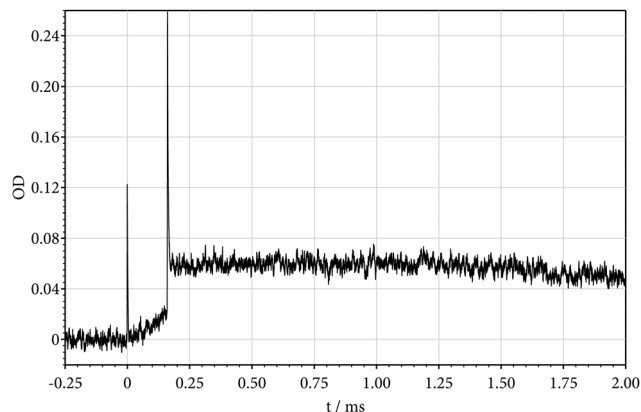
3154 | Phys. Chem. Chem. Phys., 2017, 19, 3151–3158

This journal is © the Owner Societies 2017

Fig. 7 Absorption–time profile of $CF_2$ from $C_3F_6O$ dissociation behind incident shock wave ($T_2$ = 770 K, $[Ar]_2$ = 2.1 × $10^{-5}$ mol cm$^{-3}$) and further heating $CF_3COF + CF_2$ by a reflected shock wave ($T_5$ = 1382 K, $[Ar]_5$ = 4.5 × $10^{-5}$ mol cm$^{-3}$) in a low-concentration experiment ($[C_3F_6O]_{t=0}/[Ar]$ = 4.0 × $10^{-5}$).

reaction (1). The $CF_2$ yield directly behind the reflected shock wave between 1000 K and 2000 K increases with temperature until a maximum of about $Y \approx 1.7$ is approached such as also demonstrated in Fig. 6.

Compared to the low concentration situation of Fig. 7, the situation changed when higher reactant concentrations like 530 ppm $C_3F_6O$ in Ar were investigated. Fig. 8 shows an example. In this case, $CF_2$ formation by reaction (1) is followed by dimerization (3) behind the incident shock wave. $C_2F_4$ from dimerization (3) decomposes nearly instantaneously by reaction (2) at a temperature of 1736 K of the reflected wave. After this, one observes a further increase of $CF_2$ on a time scale of 10 μs before some $CF_2$ is consumed and a final much slower further increase of $CF_2$ sets in. We note that no other absorption than that of $CF_2$ is observable under our conditions. We also note that a $CF_2$ yield of unity in Fig. 8 corresponds to OD = $\varepsilon \cdot x \cdot [CF_2]$ = 0.4. Like in Fig. 6 and 7 there is hence additional $CF_2$ formation behind



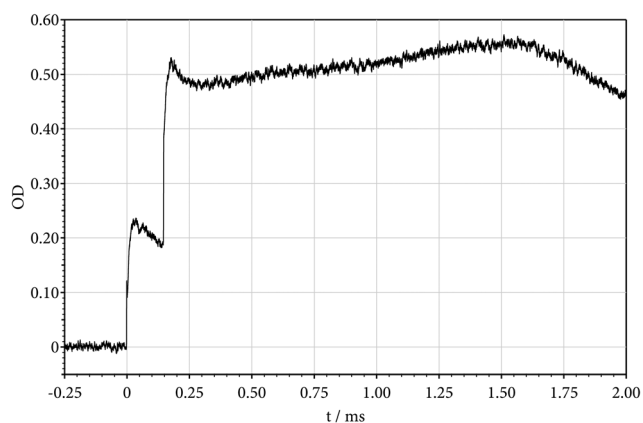Fig. 8 As Fig. 6, in a high-concentration experiment ($[C_3F_6O]_{t=0}/[Ar]$ = 5.3 × $10^{-4}$). The $CF_2$ signal behind the incident wave ($T_2$ = 918 K, $[Ar]_2$ = 1.4 × $10^{-5}$ mol cm$^{-3}$) shows $C_3F_6O$ decomposition and $CF_2$ dimerization; the $CF_2$ signal behind reflected wave ($T_5$ = 1736 K, $[Ar]_5$ = 2.9 × $10^{-5}$ mol cm$^{-3}$) shows the influence of reaction (6) followed by reactions (13)–(17).

the reflected wave with a concentration-independent component, determined by reactions (5) and (6), and concentration-dependent subsequent kinetics. These observations will be further rationalized below on the basis of the calculated energetics of various pathways. The fact that the increase and decrease of $CF_2$ during the first 100 μs behind the reflected shock in Fig. 8 were not observed in low-concentration experiments like Fig. 7 indicates that bimolecular reactions must have been involved, see below.

## 3. Calculation of energy profiles and rate constants

Like in our previous work,[8,11,13–15] we performed quantum-chemical calculations at the CBS-QB3[20] and the G4MP2[21] ab initio composite levels. The G4MP2 calculations used B3LYP/6-31G(2df,p) optimized geometries and harmonic vibrational frequencies (scaled by 0.9854). In order to study the influence of the basis set on these properties, additional calculations with the larger basis set B3LYP/6-311+G(3df) were also carried out. The Gaussian 09 software[22] was employed for all calculations. Conventional transition state theory was used to calculate limiting high pressure rate constants for rigid activated complexes. In the case of simple bond scissions with loose activated complexes, statistical adiabatic channel model calculations with a standard parameter $\alpha/\beta \approx 0.5$ were employed.[23] Limiting low pressure rate constants were estimated according to the method of ref. 24. Falloff curves were modelled following the method obtained in ref. 24–26.

First, the calculations for reaction (1) are described. The relevant decomposition pathway $C_3F_6O \rightarrow CF_3COF + CF_2$ was confirmed to involve a rigid transition state of the $CF_3C(O)FCF_2$ structure such as illustrated in Fig. 9. After this structure has been reached, the system decomposes directly to $CF_3COF + CF_2$. The enthalpies (at 0 K, in kJ mol$^{-1}$) of the transition state and of the final products at different levels of theory were found to be (161.1, 156.1, 156.1) and (123.0, 108.4, 107.9), resp., for calculations with model a = CBS-QB3, model b = G4MP2, and model c = G4MP2//B3LYP/6-311+G(3df) methods. The molecular parameters at the three levels of theory are summarized in the Appendix. The corresponding limiting high pressure rate constants in the form of $k_{1,\infty} = A_{1,\infty} \exp(-E_{a,1}/RT)$ s$^{-1}$ were found to be represented by $A_{1,\infty}$ = (2.8 × $10^{14}$, 2.8 × $10^{14}$, 3.0 × $10^{14}$) s$^{-1}$, and $E_{a,1}$ = (167.8, 162.8, 162.8) kJ mol$^{-1}$ for the models (a, b, c). Previous work gave experimental values of $A_{1,\infty}$ = (1.6 × $10^{13}$, 6.3 × $10^{13}$, 1.3 × $10^{14}$) s$^{-1}$ and $E_{a,1}$ = (151.9, 153.1, 161.9) kJ mol$^{-1}$ in ref. 5, 6, 7 respectively. The agreement between the previous experimental results and the present calculations, e.g. is illustrated by $k_1$(750 K) = (4.2 × $10^2$, 1.4 × $10^3$, 8.5 × $10^2$, 5.7 × $10^2$, 1.3 × $10^3$, 1.4 × $10^3$) s$^{-1}$ for ref. 5, 6, 7, model a, model b, and model c. The experimental result from the present work, such as given by eqn (10) was $k_1$(750 K) = 5.6(±1) × $10^2$ s$^{-1}$ which is well consistent with the previous experiments and the model calculations. Modelling of the falloff curves of reaction (1) indicated that, at the low temperatures of the present experiments and with a molecule of a size as large as $C_3F_6O$, no falloff corrections to $k_1$ were required, i.e. $k_1/k_{1,\infty} \geq 0.9$. The measured $k_1$ thus corresponds

This journal is © the Owner Societies 2017

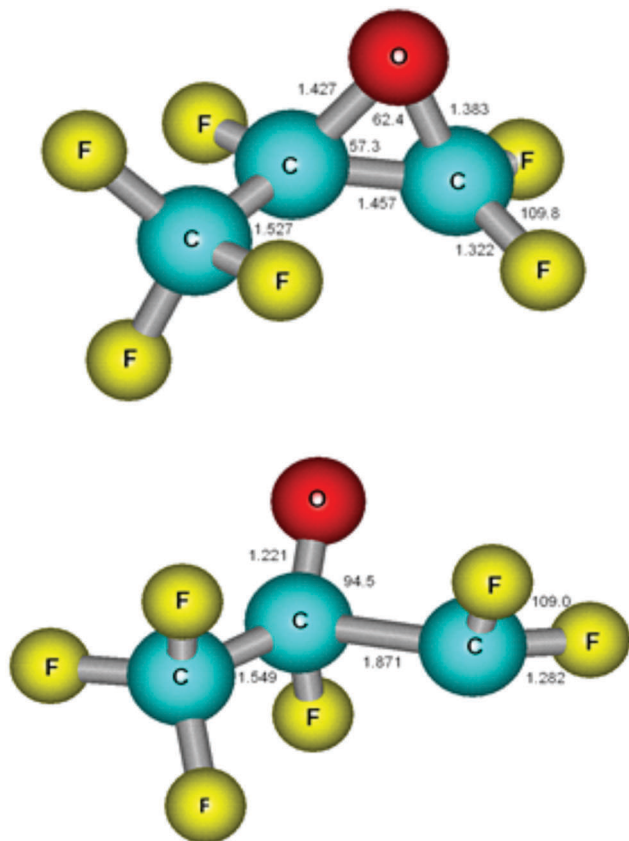Phys. Chem. Chem. Phys., 2017, 19, 3151–3158 | 3155

**Fig. 9** Structures of $C_3F_6O$ (top) and the transition state on the way to $CF_3COF + CF_2$ (bottom): calculations at the B3LYP/6-31G(2df,p) level, (see the text), bond lengths in Å.

to the high pressure rate constant $k_{1,\infty}$. This result is perfectly in line with the results for the decomposition of $c$-$C_3F_6$ such as investigated in ref. 8.

Next we inspect the thermal decomposition of $CF_3COF$, on which nothing was known from previous work. As our experiments only provided limited information, theoretical modelling of the reaction and its pathways proved most helpful. For this reaction we again did G4MP2 calculations such as characterized above. The derived energy parameters are summarized in Table 3. Obviously, pathways (5) and (6) appear most favourable, while pathway (7) as well as the pathways leading to O atoms can be ruled out on energetic reasons. Calculated molecular parameters are given again in the Appendix. In this case, modelling of the kinetics between 1400 and 1900 K led to

$$k_{5,\infty} = 7.1 \times 10^{14} \exp(-320 \text{ kJ mol}^{-1}/RT) \text{ s}^{-1} \quad (11)$$

$$k_{6,\infty} = 3.9 \times 10^{15} \exp(-355 \text{ kJ mol}^{-1}/RT) \text{ s}^{-1} \quad (12)$$

The difference in the preexponential factors reflects the fact that reaction (5) has a more rigid transition state than reaction (6). Because $CF_3COF$ is smaller than $C_3F_6O$ and the temperatures of interest are higher than for $C_3F_6O$, one has to expect some falloff reductions of $k_5$ and $k_6$ below the high pressure values. This was observed in our experiments as illustrated in Section 2.2. This behaviour is analogous to the dissociations of $C_2F_4$ and

**Table 3** Calculated energy barriers (on the G4MP2 *ab initio* composite level with B3LYP/6-31G(2df,p) optimized geometries, harmonic vibrational frequencies scaled by 0.9854, and single-point post-Hartree–Fock *ab initio* calculations, an average absolute energy uncertainty of 4.4 kJ mol$^{-1}$)

| Reaction | | $\Delta H_0^{\circ}/\text{kJ mol}^{-1}$ | $\Delta H_0^{\circ \neq}/\text{kJ mol}^{-1}$ |
|---|---|---|---|
| $C_3F_6O \rightarrow CF_3COF + CF_2$ | (1) | 108.4 | 156.1 |
| $CF_3COF \rightarrow COF_2 + CF_2$ | (5) | 212.5 | 293.7 |
| $CF_3COF \rightarrow FCO + CF_3$ | (6) | 360.2 | 360.2 |
| $CF_3COF \rightarrow CF_3CO + F$ | (7) | 479.5 | — |
| $CF_3COF \rightarrow C_2F_4 + O$ | | 591.2 | — |
| $CF_3COF \rightarrow CF_3CF + O$ | | 748.1 | — |
| $CF_3COF + CF_2 \rightarrow CF_3CO + CF_3$ | | 128.9 | — |
| $FCO \rightarrow CO + F$ | (14) | 138.5 | 138.5 |
| $CF_3 \rightarrow CF_2 + F$ | (17) | 350.6 | 350.6 |

$C_2F_6$ in ref. 11 and 19, resp. The present calculations also strongly suggested that $CF_3COF$ decomposition proceeds on the two pathways (5) and (6) while other dissociations should be of only very minor importance. More details of the falloff curves of reactions (5) and (6) are given in the Appendix.
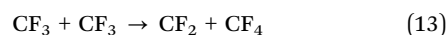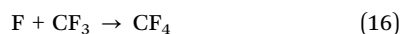
## 4. Discussion

In contrast to the dissociation of $c$-$C_3F_6$, where an intermediate 1,3 biradical $CF_2CF_2CF_2$ (the "bond-stretched invertomer" of ref. 27) with an energy minimum is passed before the rate-determining energy barrier is reached, we did not find such an energy minimum near to the transition state structure $CF_3COFCF_2$ of Fig. 9 for $C_3F_6O$ dissociation. In any case, $c$-$C_3F_6$ and $C_3F_6O$ decomposition both are convenient $CF_2$ sources releasing $CF_2$ with comparably small energy requirements. Accidentally the rate constants are very similar, with preexponential factors of $A_{1,\infty} \approx 2 \times 10^{14} \text{ s}^{-1}$ and activation energies of $E_{a,1} \approx 170 \text{ kJ mol}^{-1}$. In both cases the primary decomposition may be followed by $CF_2$ dimerization leading to $C_2F_4$ and the values for $k_3$, obtained in the present work and in ref. 8, were found to agree. The corresponding results were discussed before[8,11] and need not to be considered here, again.

While our low temperature experiments led to mixtures of $CF_3COF + (CF_2, 1/2C_2F_4)$ of 1:1 composition, the further heating of this mixture in reflected shock waves led to a more complicated picture. Consistent with our calculations, part of $CF_3COF$ decomposes to $CF_2 + COF_2$ on a time scale not much slower than that of $C_2F_4$ dissociation.[11] $COF_2$ then is thermally much more stable.[28] Reaction (5), therefore, could clearly be made responsible for an increase of the $CF_2$ yield in low-concentration experiments like Fig. 7 as well as in the time-resolved experiments like Fig. 6. The high-concentration experiments of Fig. 8, however, revealed a more complicated mechanism of secondary reactions. We interpret the additional $CF_2$ signals by a reaction sequence which is initiated by the dissociation channel (6) of $CF_3COF$, *i.e.*

$$CF_3COF \rightarrow CF_3 + FCO \quad (6)$$

which is then followed by

$$CF_3 + CF_3 \rightarrow CF_2 + CF_4 \quad (13)$$

$$FCO \rightarrow CO + F \tag{14}$$

$$F + CF_2 \rightarrow CF_3 \tag{15}$$

$$F + CF_3 \rightarrow CF_4 \tag{16}$$

$$CF_3 \rightarrow CF_2 + F \tag{17}$$

Further reactions like $CF_3COF \rightarrow CF_3CO + F$, $CF_3CO \rightarrow CF_3 + CO$ according to Table 3 should be of only minor importance. We note that FCO and $CF_3CO$ are thermally very unstable,[29,30] while $CF_4$ decomposition requires much higher temperatures to occur.[31] The rate constants of reactions (15) and (16) are known.[19,31] On their basis one concludes that these reactions influence the partial balance between $CF_3$ formation and consumption in a subtle way. Our observation of a marked concentration dependence of the $CF_2$ signals in Fig. 7 and 8 calls for a bimolecular $CF_2$-forming reaction which we suggest to be reaction (13). So far nothing has been known on this disproportionation reaction. However, it is able to explain the additional $CF_2$ formation shortly behind the reflected wave in Fig. 8 which then should be followed by $CF_2$ consumption through reaction (15) as long as F atoms are available. All fine details of our $CF_2$ signals in Fig. 8 could be reproduced by the described mechanism. However, because of the complexity of the mixture it did not appear warranted to further deduce rate constants from this analysis. Experiments with more specific precursors would appear more suitable for this purpose.

In summary, the present work provided experimental and theoretical insights into the $CF_2$-forming decomposition of $C_3F_6O$. Using this reaction as a precursor for $CF_3COF$ formation, we were also able to shed light on the decomposition of $CF_3COF$. While the former is a simple single-channel process, the latter was shown to be dominated by the two channels (5) and (6). Although $C_3F_6O$ and $c$-$C_3F_6$ decomposition have very similar rate constants for $CF_2$ formation, their intermediates are suggested to be of different character, of $CF_3C(O)FCF_2$ ketene-form in the former and of 1,3 biradical-form $CF_2CF_2CF_2$ in the latter case. Like in fluorocarbons and hydrofluorocarbons, for the present fluorocarbon oxygenates we observed rigid activated complex elimination processes (reactions (1) and (5)) and bond scission processes with looser activated complexes (reaction (6)). Unravelling these processes is made possible by the combination of kinetics experiments and rate theories.

## Appendix

1. For molecular parameters of $C_3F_6O$ (calculated on the G4MP2//B3LYP/6-311+G(3df,3pd) level), see the text.

Vibrational frequencies (in $cm^{-1}$): 47, 133, 158, 249, 265, 306, 348, 425, 504, 535, 565, 577, 612, 722, 771, 807, 1015, 1131, 1154, 1181, 1203, 1256, 1340, 1538.

Vibrational frequencies for the transition state (in $cm^{-1}$): 297i, 50, 70, 112, 172, 227, 243, 299, 377, 384, 454, 537, 587, 665, 678, 733, 809, 1035, 1185, 1194, 1263, 1291, 1304, 1673.

Rotational constants (in $cm^{-1}$): 0.0737, 0.0364, 0.0310.

Rotational constants for the transition state (in $cm^{-1}$): 0.0674, 0.0350, 0.0305.

2. For molecular parameters of $CF_3COF$ (calculated on the G4MP2//B3LYP/6-31+G(2df,p) level), see the text.

Vibrational frequencies (in $cm^{-1}$): 45, 219, 229, 377, 417, 508, 583, 683, 758, 801, 1108, 1196, 1251, 1318, 1928.

Vibrational frequencies for the transition state of reaction (5) (in $cm^{-1}$): 305i, 83, 145, 146, 347, 421, 527, 580, 673, 723, 766, 1001, 1344, 1377, 1822, (the torsion is treated as a free rotor).

Rotational constants (in $cm^{-1}$): 0.128, 0.0831, 0.0687.

Rotational constants for the transition state of reaction (5) (in $cm^{-1}$): 0.132, 0.0767, 0.0640.

3. Modelling of falloff curves for the dissociation reactions

$$CF_3COF \rightarrow CF_2 + COF_2 \tag{5}$$

and

$$CF_3COF \rightarrow CF_3 + FCO \tag{6}$$

Calculations with modelled high pressure rate constants of eqn (11) and (12) and low pressure rate constants

$$k_{5,0} = [Ar]9.0 \times 10^{21}(T/1600 \text{ K})^{-13.6} \exp(-339 \text{ kJ mol}^{-1}/RT)$$
$$\text{cm}^3 \text{ mol}^{-1} \text{ s}^{-1}$$

$$k_{6,0} = [Ar]7.2 \times 10^{22}(T/1600 \text{ K})^{-13.6} \exp(-394 \text{ kJ mol}^{-1}/RT)$$
$$\text{cm}^3 \text{ mol}^{-1} \text{ s}^{-1}$$

The modelling assumed a temperature-independent average energy transferred per collision of $\langle \Delta E \rangle/hc = -100 \text{ cm}^{-1}$ which led to low pressure collision efficiencies $\beta_c$ of 0.046, 0.039, and 0.029 for reaction (5) and 0.051, 0.044, and 0.033 for reaction (6) at $T = 1400$, 1550, and 1850 K, respectively. The falloff curves were constructed following the method of ref. 24–26. The falloff curves obtained are illustrated in Fig. 10. They can be represented
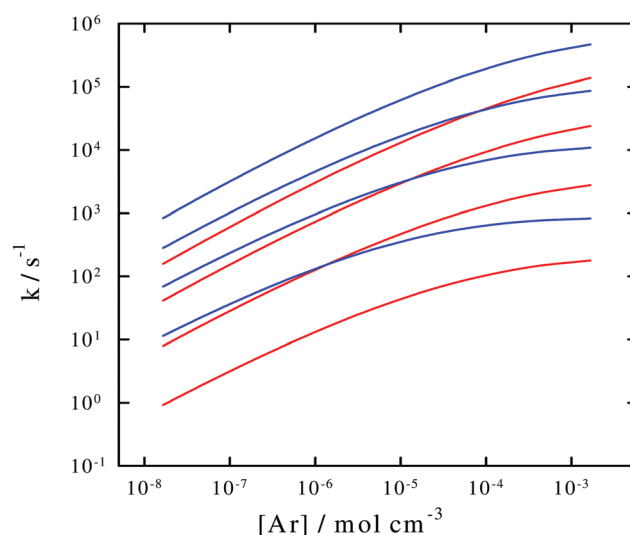


**Fig. 10** Modelled falloff curves for $CF_3C(O)F \rightarrow COF_2 + CF_2$ (in blue) and $CF_3C(O)F \rightarrow CF_3 + FCO$ (in red). Calculations for 1400, 1550, 1700 and 1850 K (from bottom to top), using rate coefficients described in the Appendix.

in the format of ref. 26 with center broadening factors of $F_{cent}$ = 0.064, 0.065, and 0.070 for reaction (5) and 0.055, 0.053, and 0.053 for reaction (6) at $T$ = 1400, 1550, and 1850 K, respectively.

## Acknowledgements

## References

1  D. R. Burgess, M. R. Zachariah, W. Tsang and P. R. Westmoreland, *Prog. Energy Combust. Sci.*, 1996, **21**, 453–529.
2  P. B. Sargeant, *J. Org. Chem.*, 1970, **3**, 678–682.
3  P. B. Sargeant and C. G. Krespan, *J. Am. Chem. Soc.*, 1969, **91**, 415–419.
4  W. Mahler and P. R. Resnick, *J. Fluorine Chem.*, 1973/74, **3**, 451–452.
5  R. C. Kennedy and J. B. Levy, *J. Fluorine Chem.*, 1976, **7**, 101–114.
6  Yu. N. Zhitnev, V. V. Timofeev and N. Yu. Ignat'eva, *High Energy Chem.*, 1994, **28**, 484–491.
7  P. J. Krusic, D. C. Roe and B. E. Smart, *Isr. J. Chem.*, 1999, **39**, 117–123.
8  C. J. Cobos, L. Sölter, E. Tellbach and J. Troe, *J. Phys. Chem. A*, 2014, **118**, 4873–4879.
9  W. J. R. Tyerman, *J. Chem. Soc., Faraday Trans.*, 1969, **65**, 1188–1198.
10  F. Battin-Leclerc, A. P. Smith, G. D. Hayman and T. P. Murrells, *J. Chem. Soc., Faraday Trans.*, 1996, **92**, 3305–3313.
11  C. J. Cobos, A. E. Croce, K. Luther, L. Sölter, E. Tellbach and J. Troe, *J. Phys. Chem. A*, 2013, **117**, 11420–11429.
12  E. B. Aslanidi, V. T. Zarubin and Yu. S. Turishchev, *Laser Chem.*, 1986, **6**, 373–380.
13  C. J. Cobos, L. Sölter, E. Tellbach and J. Troe, *J. Phys. Chem. A*, 2014, **118**, 4880–4888.
14  C. J. Cobos, K. Hintzer, L. Sölter, E. Tellbach, A. Thaler and J. Troe, *Phys. Chem. Chem. Phys.*, 2015, **17**, 32219–32224.
15  C. J. Cobos, L. Sölter, E. Tellbach and J. Troe, *Phys. Chem. Chem. Phys.*, 2014, **16**, 9797–9807.
16  C. J. Cobos, K. Hintzer, L. Sölter, E. Tellbach, A. Thaler and J. Troe, *Phys. Chem. Chem. Phys.*, 2016, DOI: 10.1039/C6CP06822G.
17  V. A. Dunyakhin, O. V. Kuricheva, V. V. Timofeev and Yu. N. Zhitnev, *Russ. Chem. Bull.*, 1995, **11**, 2079–2086.
18  C. J. Cobos, A. E. Croce, K. Luther and J. Troe, *J. Phys. Chem. A*, 2010, **114**, 4755–4761.
19  C. J. Cobos, A. E. Croce, K. Luther and J. Troe, *J. Phys. Chem. A*, 2010, **114**, 4748–4754.
20  J. A. Montgomery, M. J. Frisch, J. W. Ochterski and G. A. Petersson, *J. Chem. Phys.*, 2007, **127**, 124105.
21  L. A. Curtiss, P. C. Redfern and K. Raghavachari, *J. Chem. Phys.*, 2007, **127**, 124105.
22  M. J. Frisch, *et al.*, *Gaussian 09, Revision A.02-SMP*, Gaussian, Inc., Wallingford, CT, 2009.
23  C. J. Cobos and J. Troe, *J. Chem. Phys.*, 1985, **3**, 1010–1015.
24  J. Troe, *J. Phys. Chem.*, 1979, **83**, 114–126.
25  J. Troe, *Ber. Bunsenges. Phys. Chem.*, 1983, **87**, 161–169.
26  J. Troe and V. G. Ushakov, *Z. Phys. Chem.*, 2014, **1**, 1–10.
27  H. Wei, D. A. Hrovat, W. R. Dolbier, B. E. Smart and W. T. Borden, *Angew. Chem., Int. Ed.*, 2007, **46**, 2666–2668.
28  A. P. Modica, *J. Phys. Chem.*, 1970, **74**, 1194–1204.
29  V. D. Knyazev, A. Bencsura and I. R. Slagle, *J. Phys. Chem. A*, 1997, **101**, 849–852.
30  A. Tomas, F. Caralp and R. Lesclaux, *Z. Phys. Chem.*, 2000, **214**, 1349–1365.
31  G. Knight, L. Sölter, E. Tellbach and J. Troe, *Phys. Chem. Chem. Phys.*, 2016, **26**, 17592–17596.